International Journal of Numerical Methods for Heat & Fluid Flow

Emerald Article: Natural convection flow under magnetic field in a square cavity for uniformly (or) linearly heated adjacent walls

M. Sathiyamoorthy, Ali J. Chamkha

The current issue and full text archive of this journal is available at
www.emeraldinsight.com/0961-5539.htm

Natural convection flow under magnetic field in a square cavity for uniformly (or) linearly heated adjacent walls

M. Sathiyamoorthy
Department of Mathematics, Government Thirumagal Mill's College, Gudiyatham, India, and
Ali J. Chamkha
Manufacturing Engineering Department, Public Authority for Applied Education and Training, Shuweikh, Kuwait

Received 6 September 2010
Revised 7 December 2010, 7 January 2011
Accepted 13 January 2011

Abstract

Purpose – The purpose of this paper is to study the effect of magnetic field on natural convection in an enclosure with uniformly or linearly heated adjacent walls and especially its effect on the local and average Nusselt numbers.

Design/methodology/approach – The problem is formulated and solved using the finite element method. Accuracy of the method is validated by comparisons with previously published work.

Findings – It was found that the presence of a magnetic filed causes significant effects on the local and average Nusselt numbers on all considered walls.

Originality/value – Although the problem is not very original it is important in that many applications have heating on adjacent walls.

Keywords MHD convective flow, Liquid metals, Non-uniform heating, Convection, Magnetic fields

Paper type Research paper

Nomenclature

$\bar{B}$ = applied magnetic field
B = magnitude of magnetic field
g = acceleration due to gravity, $\mathrm{m\,s^{-2}}$
L = side of the square cavity, m
Nu = local Nusselt number
$\overline{Nu}$ = average Nusselt number
Ha = Hartmann number
p = pressure, Pa
P = dimensionless fluid pressure
Pr = Prandtl number
Ra = Rayleigh number
T = fluid temperature, K
T_c = temperature of cold walls, K
T_h = temperature of hot walls, K
ux = component of velocity
Ux = component of dimensionless velocity
vy = component of velocity
Vy = component of dimensionless velocity
X = dimensionless distance along x coordinate
Y = dimensionless distance along y coordinate

Greek symbols

α = thermal diffusivity, $\mathrm{m^2\,s^{-1}}$
β = volume expansion coefficient, $\mathrm{K^{-1}}$

The first author wishes to thank the Management of SSN College of Engineering for providing the necessary facility to carry out the present work.

International Journal of Numerical Methods for Heat & Fluid Flow
Vol. 22 No. 5, 2012
pp. 677-698

0961-5539
DOI 10.1108/09615531211231307

γ = penalty parameter
σ = electrical conductivity, $\Omega^{-1}\,m^{-1}$
θ = dimensionless temperature
ν = kinematic viscosity, $m^2 s^{-1}$
ρ = density, $kg\,m^{-3}$
ψ = stream function
ϕ = inclined angle

Subscripts
b = bottom wall
c = cooled wall
h = hot wall
l = left wall
r = right wall
s = side wall
t = top wall

1. Introduction

Natural convection of an electrically conducting fluid in a magnetic field have been studied in resent years by several authors. Because the process of manufacturing materials in industrial problems and microelectronic heat transfer devices involve an electrically conducting fluid subjected to magnetic field. In this case the electrically conducting fluid experiences a Lorentz force and its effect is to reduce the flow velocities which turn the affects in the heat transfer rate. Study and thorough understanding of the momentum and heat transfer in such process is important for the better control and quality of manufactured products. A comprehensive literature survey concerned with this subject is given by Yang (1987), Kulacki *et al.* (1987), Moreau (1990), Utech and Flemmings (1966), Vives and Perry (1987) and Series and Hurle (1991).

The literature survey shows that Oreper and Szekely (1983), Ozoe and Maruo (1987), Ozoe and Okada (1989), Garandet *et al.* (1992) and Venkatachalappa and Subbaraya (1993) have made attempts to acquire a basic understanding of flows and heat transfer characteristics in an enclosure in the presence of magnetic field. They found that the magnetic field slow downs the movement of the fluid and decreases the heat transfer rate in the enclosures. The study of Oreper and Szekely (1983) shows that the strength of magnetic filed is one of the most important factors for crystal formation. Rudraiah *et al.* (1995) and Alchaar *et al.* (1995) have shown a specific interest to focus on a natural convection within a rectangular enclosure with a magnetic field where one vertical wall is cooled and another one heated while the remaining top and bottom walls are well insulated. Ece and Buyuk (2006) illustrated the natural convection flow under a magnetic field in a inclined rectangular cavity for heated and cooled on the adjacent walls while differentially heated and isolated opposite walls investigated by Pirmohammadi and Ghassemi (2009). Mahmud and Fraser (2004) have investigated magneto hydrodynamic natural convection flow and entropy generation in a square cavity. Recently, Kahveci and Oztuna (2009) have investigated MHD natural convection flow and heat transfer in a laterally heated partitioned enclosure. In most of the previous studies, isothermal or isoflux thermal boundary conditions was applied to side walls of enclosures. For non-isothermal boundary conditions, Oztop *et al.* (2009) have investigated numerical simulation of magneto hydrodynamic buoyancy flow in a enclosure when the bottom wall is non-uniformly heated while the top wall is non-uniformly heated investigated by Kakarantzas *et al.* (2009). Sathiyamoorthy and Chamkha (2009) have also studied when the side walls are linearly heated. In the mixed convection flow, Sivasankaran *et al.* (2011) have studied hydro-magnetic combined convection in a lid-driven cavity with sinusoidal boundary conditions on both sidewalls.

The present paper investigates the effect of magnetic field on natural convection flow within a square cavity filled with liquid metals when the bottom and left walls

are uniformly (constant temperature) or linearly heated while the right and top walls are cooled. In the case of uniformly heated bottom and left walls, two discontinuity appearers in temperature distribution, one at the right edge of bottom wall and another at left edge of top wall. These discontinuity can be removed by considering the linear temperature profile on the walls. The main object is to determine the influence of Hartmann number with inclined angles on the circulations, temperature distributions within the cavity and heat transfer rates at the heated walls in terms of Nusselt numbers.

2. Mathematical formulation

Consider a square cavity filled with viscous, incompressible and electrically conducting fluid which is permeated by a uniform magnetic field $\bar{B}$ with magnitude B at an inclined angle ϕ from the horizontal plane (Figure 1). The Boussinesq approximation is invoked for the fluid properties to relate density changes to temperature changes. The viscous, radiation and Joule heating effects are neglected. The magnetic Reynolds number is assumed to be small so that the induced magnetic field is neglected. Under the above assumption, the conservation equations for momentum and electric transfer are given by:

$$(\bar{V}.\nabla)\bar{V} = -\frac{1}{\rho}\nabla p + \nu\nabla^2\bar{V} + \frac{\bar{J}}{\rho}\times\bar{B} - \beta(T - Tc)\bar{g} \tag{1}$$

$$\bar{J} = \sigma(-\nabla\varphi + \bar{V}\times\bar{B}) \tag{2}$$

$$\nabla^2\bar{\varphi} = \bar{B}.\omega, \quad \omega = \nabla\times\bar{V}. \tag{3}$$

where $\bar{V}$ is the fluid velocity vector, ω is vorticity field, T is the fluid temperature, p is pressure, $\bar{B}$ is the external magnetic field, $\bar{J}$ is the electric current, φ is the electric

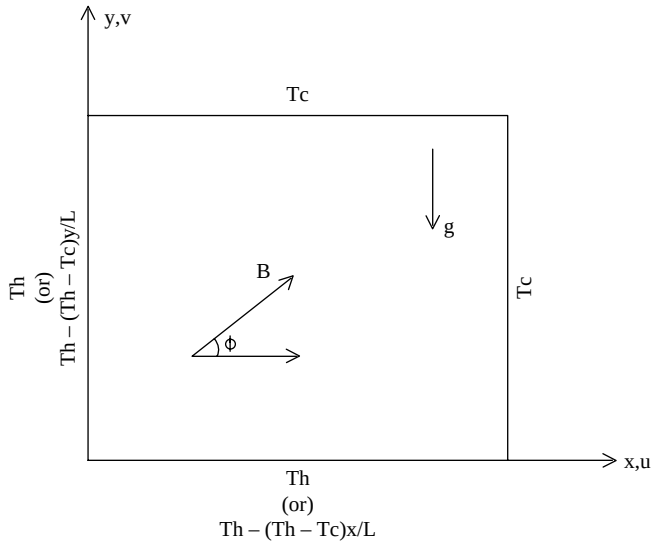

Figure 1.
Schematic diagram of the physical system of the present problem

potential, σ is electric conductivity and $-\nabla\varphi$ is associated electric field. As discussed by Sreenivasan *et al.* (2005) for the case of a steady and two-dimensional flow where the magnetic field lies in the plane of motion, equation (3) reduces to $\nabla^2\varphi = 0$, and provided the fluid is bounded by perfectly conducting walls that provide a resistance-free path from induced current. It follows that the electric field vanishes everywhere in the cavity. Under these conditions the dimensionless governing equations for the steady natural convection flow can be written as:

$$\frac{\partial U}{\partial X} + \frac{\partial V}{\partial Y} = 0 \tag{4}$$

$$U\frac{\partial U}{\partial X} + V\frac{\partial U}{\partial Y} = -\frac{\partial P}{\partial X} + Pr\nabla^2 U + PrHa^2(V\sin\phi\cos\phi - U\sin^2\phi) \tag{5}$$

$$U\frac{\partial V}{\partial X} + V\frac{\partial V}{\partial Y} = -\frac{\partial P}{\partial Y} + Pr\nabla^2 V + PrHa^2(U\sin\phi\cos\phi - V\cos^2\phi) + RaPr\theta \tag{6}$$

$$U\frac{\partial \theta}{\partial X} + V\frac{\partial \theta}{\partial Y} = \left(\frac{\partial^2\theta}{\partial X^2} + \frac{\partial^2\theta}{\partial Y^2}\right). \tag{7}$$

The following change of variables are implemented in the above equations:

$$X = \frac{x}{L},\ \ Y = \frac{y}{L},\ \ U = \frac{uL}{\alpha},\ \ V = \frac{vL}{\alpha},\ \ \theta = \frac{T - T_c}{T_h - T_c},$$

$$P = \frac{pL^2}{\rho\alpha^2},\ \ Pr = \frac{v}{\alpha},\ \ Ra = \frac{g\beta(T_h - T_c)L^3Pr}{\nu^2},\ \ Ha = LB\sqrt{\frac{\sigma}{\mu}}. \tag{8}$$

The boundary conditions in the present study as follows:

$$\begin{aligned} &U(X,0) = U(X,1) = U(0,Y) = U(1,Y) = 0;\\ &V(X,0) = V(X,1) = V(0,Y) = V(1,Y) = 0;\\ &\theta(X,0) = 1 \text{ or } 1 - X, \theta(0,Y) = 1 \text{ or } 1 - Y;\\ &\theta(1,Y) = 0,\ \ \theta(X,1) = 0. \end{aligned} \tag{9}$$

3. Numerical method and validation

In order to determine the flow and heat transfer in the cavity the penalty finite element method is used to solve the non-dimensional governing equations (4)-(7) along with the boundary conditions (9). In this method nine nodebi-quadratic elements are used to get smooth solutions. The full details of this method can be found in Reddy and Gartling (1994) and a brief description is given in the Appendix. The numerical solutions are obtained in terms of velocity components (U, V) and temperature (θ). The fluid motion is displayed using the stream function (ψ) obtained from the velocity components U and V. The relationship between the stream function and velocity components flows are $U = (\partial\psi/\partial Y)$ and $V = -(\partial\psi/\partial X)$, which yields a single poisson equation:

$$\frac{\partial^2 \psi}{\partial X^2} + \frac{\partial^2 \psi}{\partial Y^2} = \frac{\partial U}{\partial Y} - \frac{\partial V}{\partial X}(vorticity). \tag{10}$$

It is known as the positive sign of ψ denotes anticlockwise circulation while the negative sign connotes the clockwise circulation. The Galerikin finite element method is used to solve the linear equation (10). The no-slip condition is valid at all boundaries as there is no cross flow, hence $\psi = 0$ is used for the boundaries.

The heat transfer coefficient in terms of the local Nusselt number is defined by:

$$Nu = -\left.\frac{\partial \theta}{\partial n}\right|_{Wall}, \tag{11}$$

where n-denotes the normal direction on a plane. The local Nusselt number at the horizontal walls (Nu_h) and the side walls (Nu_s) are evaluated for various wall boundary conditions using the above definition. The average Nusselt numbers at the horizontal and side walls are computed as follows:

$$\overline{Nu_h} = \int_0^1 Nu_h dX \text{ and } \overline{Nu_s} = \int_0^1 Nu_s dY. \tag{12}$$

The computational domain consists of 20×20 bi-quadratic elements which correspond to 41×41 grid points. In order to verify the accuracy of the numerical procedure we have compared the obtained results for the case when magnetic field absent ($Ha = 0$) with benchmark solution of Mallinson and Vahl Davis (1977). Further, a second test concerned with magnetic field which has been investigated by Rudraiah *et al.* (1995). The results were in well agreement as seen in Table I. Computations have been carried out for various values of $Ha = 0$-100 and $\phi = 0,(\pi/2)$ for $Ra = 10^5$ and $Pr = 0.054$ (liquid metals) with uniformly or linearly heated bottom and left walls and cooled right and top walls.

4. Results and discussions

1. Streamlines and isotherms

1. Uniformly heated adjacent walls.

In the absence of magnetic field. Figure 2 show the streamlines and isotherms for uniformly heated left and bottom walls and cooled right and top walls for $Ra = 10^5$ and $Pr = 0.054$ in the absence of magnetic field ($Ha = 0$). It is clear that the flow within the cavity takes place by virtue of thermal buoyancy effects (heated and cooled adjacent walls) which is represented by the Rayleigh number Ra. As seen in Figure 2 for the

Gr	Ha	Rudraiah *et al.* (1995)	Present
2×10^4	0	2.5188	2.5439
	10	2.2234	2.2385
	100	1.0110	1.0066
2×10^5	0	4.9198	5.0245
	10	4.8053	4.9136
	100	1.4317	1.4292

Note: $Pr = 0.733$

Table I. Comparison of the predicted Nusselt number $\overline{Nu}$ on the left or right walls of the cavity with reference to Rudraiah *et al.* (1995)

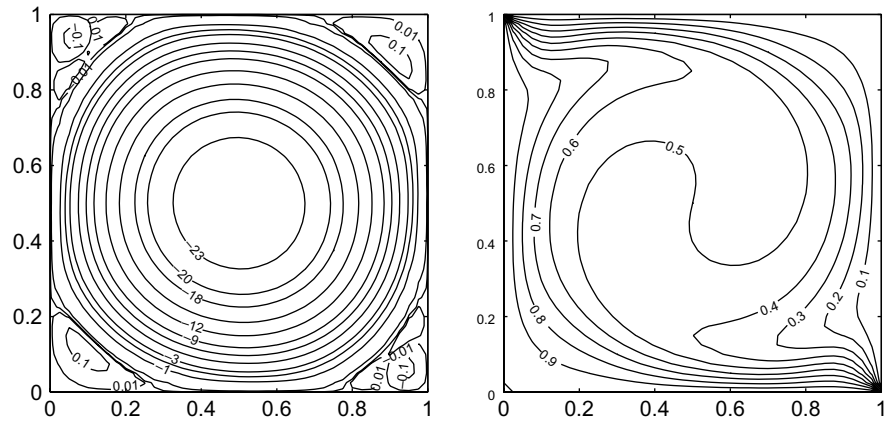

Figure 2.
Contour plots of uniformly heated left and bottom walls in the absence of magnetic field

Note: $Ha = 0$

relatively high Rayleigh number $Ra = 10^5$, the fluid rises up along the left wall and flows down along the cold right wall and forms rotating concentric circles (clockwise direction) in the cavity with center at center of the cavity. At all corners of the cavity, secondary circulating cell are formed due to thermal buoyancy effects. As expected, because the discontinuity at the left edge of the top wall and right edge of bottom wall, the variations in the temperature seems to be more in the corresponding corners of the cavity. Moreover, the isotherms $0.4 \leq \theta \leq 0.6$ covers 50 percent center portions of the cavity.

Horizontally applied magnetic field. Figure 3(a)-(c) show steady-state contour maps for the streamline and temperature for values of the Hartmann number Ha (10, 50 and 100) for $Pr = 0.054$, $Ra = 10^5$ and $\phi = 0$ (non-inclined magnetic field), respectively. The application of a transverse magnetic field in the direction of normal to the vertical walls ($\phi = 0$) has the tendency to slow down the movement of the fluid in the enclosure (Figure 3). As a result, the re-circulating cells tend to be stretched or elongated in the upward vertical direction. This process continues as the strength of the magnetic field increases until the secondary circulations that occurs all corners of the cavity disappears for $Ha = 50$ (Figure 2(b)). It is also note that the temperature profiles becomes more parallel to the side walls. Further increases in Ha(100), it is interesting to note that the fluid flow follows the parallelogram paths, i.e. the streamlines are looks like parallelograms. Also the isotherms are symmetric about the diagonal of the cavity. The braking effect of the magnetic field is observed from the maximum intensity of circulation ψ_{max}. The value of ψ_{max} for $Ha = 0$ is 25.82 while it is equal to 17.51, 4.89 and 1.19 for $Ha = 10$, 50 and 100, respectively. Temperature stratification becomes dominant as the strength of the magnetic field increases and temperature contour maps tend to become more uniform in the core region of the enclosure as Ha increases to 100 indicating the approach to a quasi-conduction regime. In addition, the magnetic field is seen to suppress the overall heat transfer in the enclosure. This suppression of convective flows by the use of magnetic fields has proven to be effective in controlling melts and has now been widely practiced in the metals semiconductor crystal growth industries (see, for instance, Series and Hurle (1991)). All of the above discussed behaviors are clearly seen in Figure 3(a)-(c).

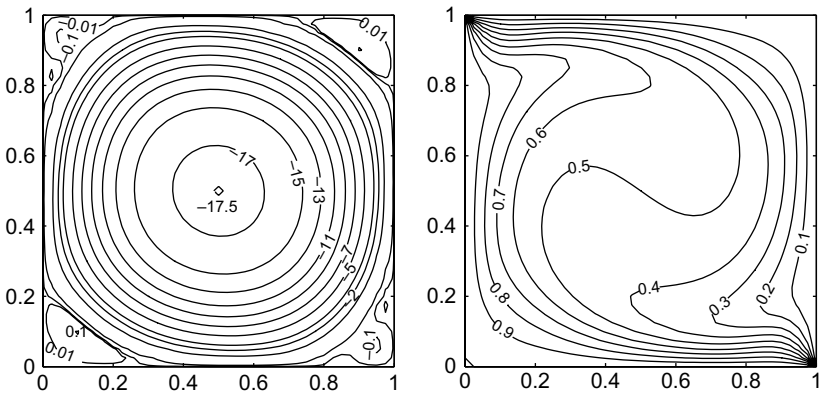

(a) Ha = 10

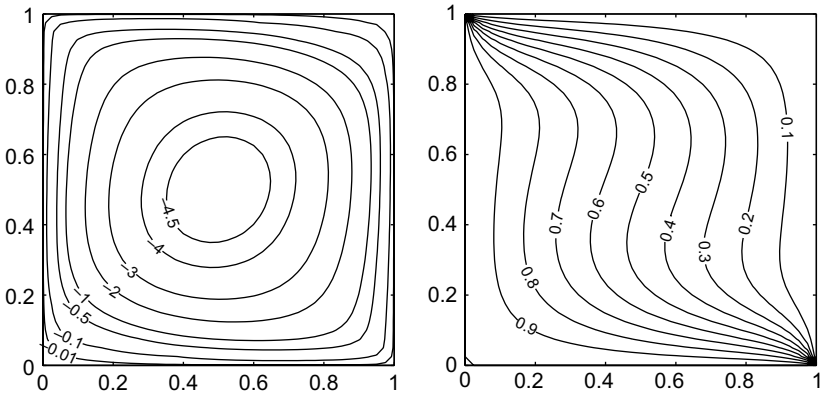

(b) Ha = 50

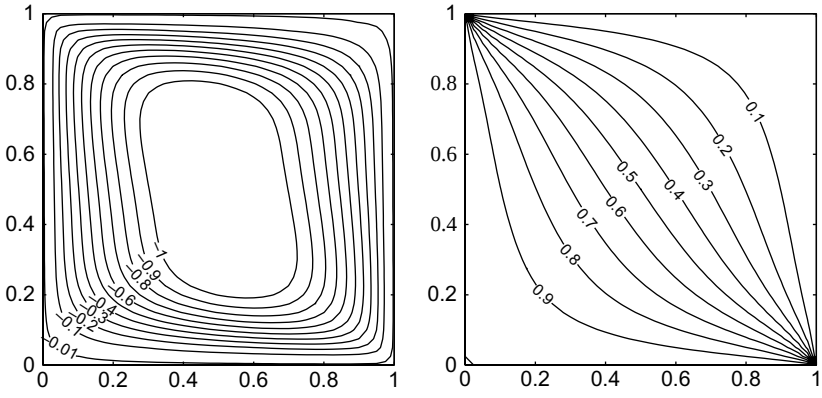

(c) Ha = 100

Note: $\phi = 0$

Figure 3.
Contour plots of uniformly heated left and bottom walls under horizontal magnetic field orientation

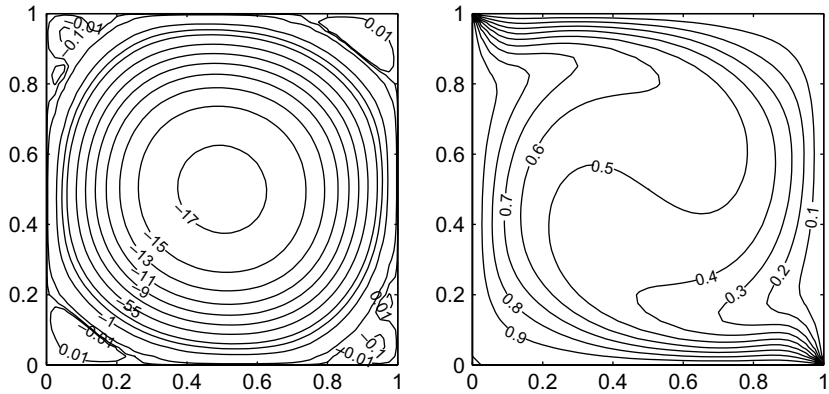

(a) Ha = 10

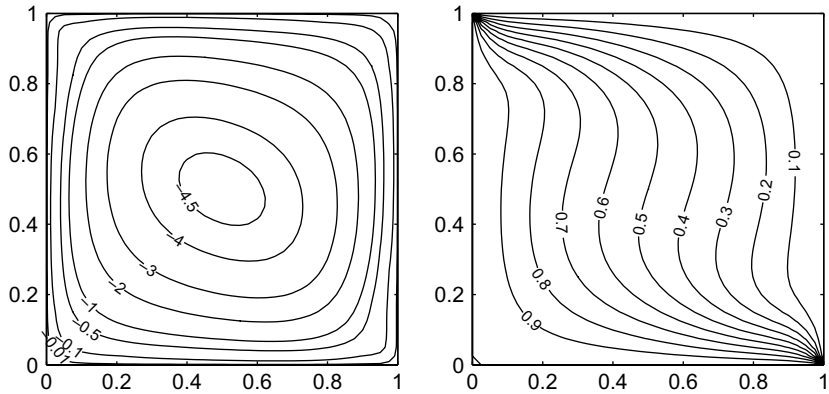

(b) Ha = 50

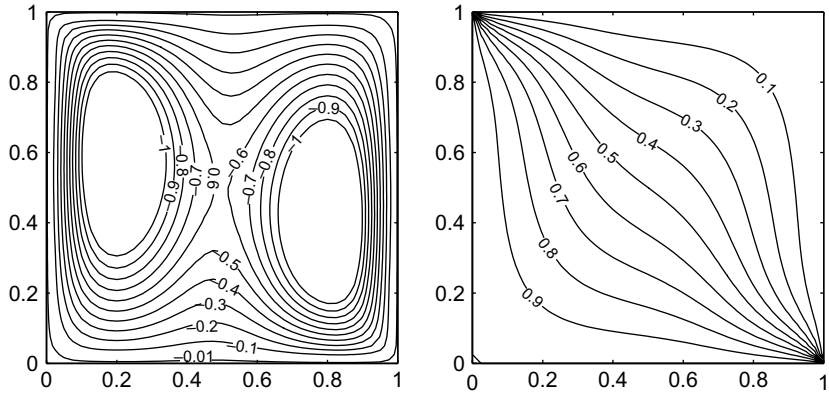

(c) Ha = 100

Note: $\phi = \pi/2$

Figure 4.
Contour plots of uniformly heated bottom and left walls under vertical magnetic field orientation

Vertically applied magnetic field. Figure 4(a)-(c) show the influence of the Hartmann number *Ha* on the streamline and isotherm contours when the magnetic field is applied in the direction normal to the horizontal walls of the enclosure ($\phi = \pi/2$) under the same conditions as Figure 3(a)-(c). For low value of $Ha = 10$, the streamlines and isotherms are more or less same for the both inclination angles $\phi = 0$ and $\pi/2$ as seen Figures 3(a) and 4(a). But as *Ha* is increased to higher values in Figure 4(b) and (c), it is observed that the primary cell is stretched along the side walls for $Ha = 50$ and it is splitted as two clockwise cells for $Ha = 100$, one cell appears near the left wall and another appears near the right wall which is contrary for the behavior of Figure 3(c). The temperature profile $\theta = 0.5$ lies almost on the diagonal of the cavity and the isotherms $\theta \geq 0.6$ lies in the left side of the diagonal and $\theta \leq 0.4$ lies right side of the diagonal. Also the isotherms $0.1 \leq \theta \leq 0.9$ spans the entire cavity. Unlike Figure 3(c) in which the isotherms are almost uniform and symmetric about the diagonal indicating quasi-conduction regime, it is shown in Figure 4(c) that even for relatively high Hartmann number $Ha = 100$, the convection regime is still dominant. This is due to the less flow retardation effect caused by the vertically applied magnetic field than the horizontally-applied one.

2. Linearly heated adjacent walls.

In the absence of magnetic field. Figure 5 show the streamlines and isotherms for linearly heated bottom and left walls for $Ra = 10^5$ and $Pr = 0.054$ in the absence of magnetic field ($Ha = 0$). It is clear that the flow pattern within the cavity same as the flow pattern for the case of uniformly heated bottom wall and left wall with lower maximum intensity of circulation ψ_{max} (Figure 2). The value of ψ_{max} is 20.27 for linearly heated walls while it is equal to 25.82 for uniformly heated walls. Contrary to the behavior of isotherms of Figure 2, it is observed that the temperature on the bottom wall and left varies linearly and it removes the discontinuity at the left and right edges of top and bottom walls. Also the temperature profiles $0.2 \leq \theta \leq 0.4$ covers large portions of the cavity.

Horizontally-applied magnetic field. Figure 6(a)-(c) shows the effects of the Hartmann number *Ha* for horizontally-applied ($\phi = 0$) magnetic fields on the contour maps of streamlines and isotherms for the case of linearly heated bottom wall left wall. As seen Figure 6(a) for $Ha = 10$, the movement of the fluid in the cavity slows down, that is the

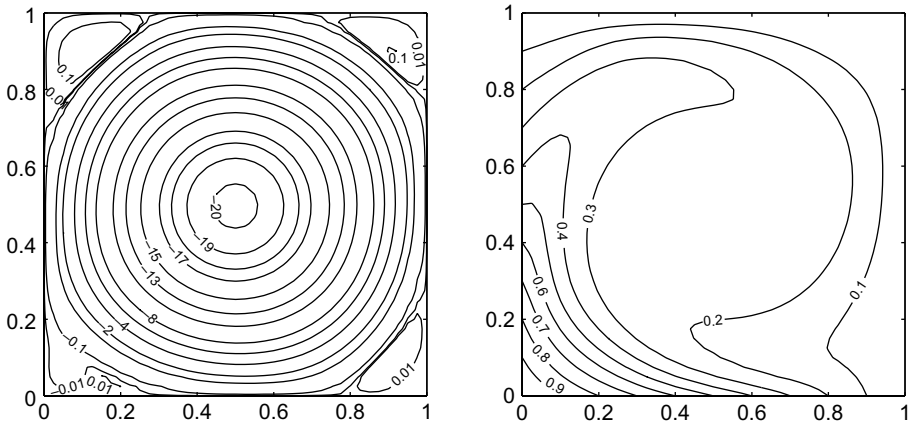

Note: $Ha = 0$

Figure 5.
Contour plots of linearly heated left and bottom walls in the absence of magnetic field

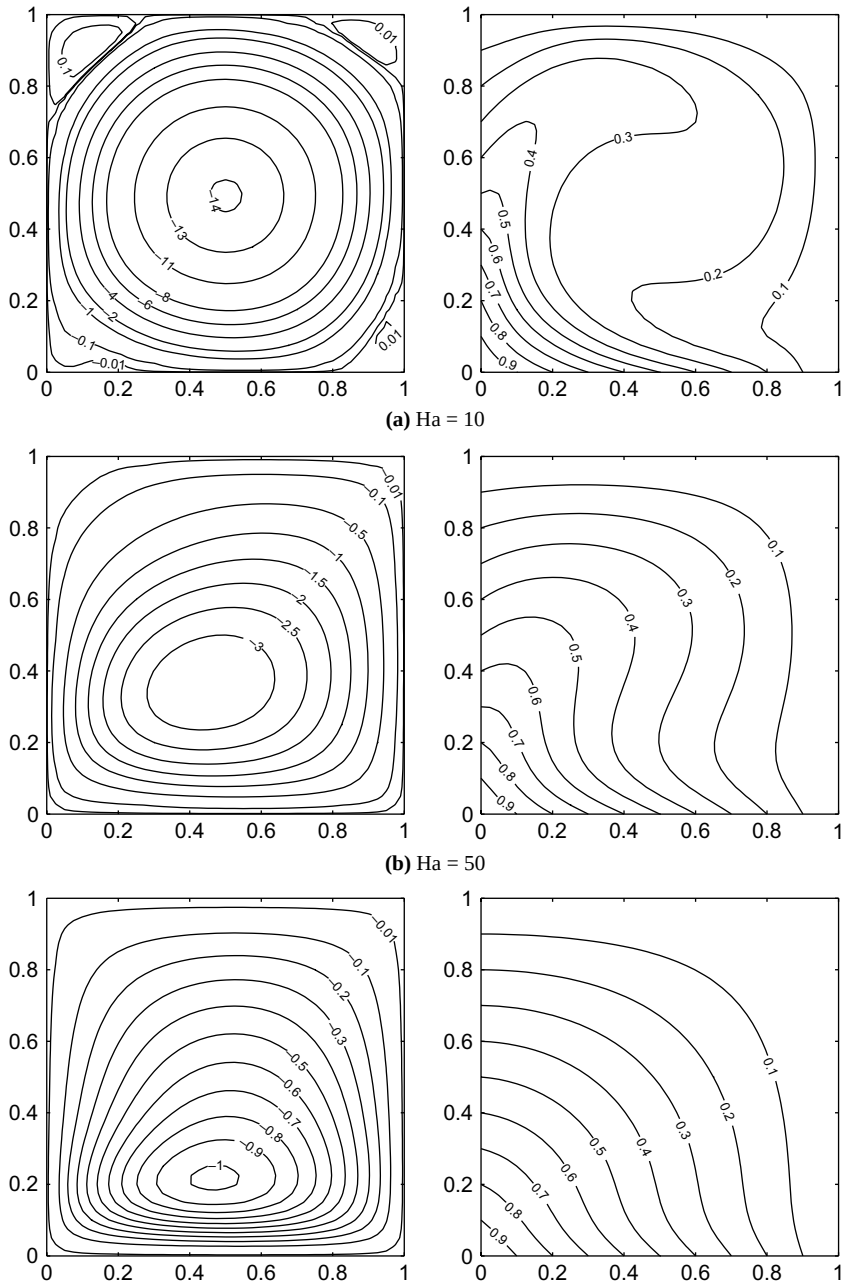

Figure 6.
Contour plots of linearly heated left and bottom walls under horizontal magnetic field orientation

Note: $\phi = 0$

strength of the primary cell and the edges at corners are reduced. Further increase in the value of *Ha* to 50, the edges at the corners are disappears and the primary circulation tend to be stretched downward towards the bottom heated wall and the temperature stratification becomes dominant. As evident from Figure 6(c), further significant increase in the value of *Ha*($Ha = 100$) causes the decrease in the circulation intensity of the primary circulation with increased stretching effect towards the bottom wall. This is represented by the movement of the core or eye of the primary cell downward closer to the linearly heated bottom wall of the cavity. Also the isotherms are almost symmetric about the diagonal of the cavity indicating the approach to a quasi-conduction regime.

Vertically applied magnetic field. Figure 7(a)-(c) shows the effects of the Hartmann number *Ha* for vertically-applied ($\phi = \pi/2$) magnetic fields on the contour maps of streamlines and isotherms under the same conditions as Figure 6(a)-(c). For $Ha = 10$, as discussed for the uniformly heated case, the effect of inclined angel is not observed (Figures 6(a) and 7(a)). Contrary to the behavior for horizontally-applied magnetic field ($\phi = 0$), as *Ha* is increased to 50 and 100 in Figure 7(a) and (b) for vertically applied magnetic field it is observed that the primary cell stretches along the linearly heated left wall respective of *Ha* and still a small edge appears at left top corner of the cavity for $Ha = 50$. It is also note that the streamlines which occurs below the eye of vortex are compressed near the bottom wall for $Ha = 100$.

2. Heat transfer rates: local and average Nusselt number

1. Uniformly heated adjacent walls. Figure 8 (a)-(d) shows the effects of the Hartmann number *Ha* and the magnetic field inclination angle ϕ on the variation of the local Nusselt number at the bottom, left, right and top walls (Nu_b, Nu_l, Nu_r, Nu_t) for the case of uniformly heated adjacent walls. As seen Figure 8(a) the heat transfer rate at the left edge of the bottom wall ($X = 0$) is 0. This is expected due to the left wall is uniformly heated. In general, it is clearly observed that the local Nusselt number at the bottom wall (Nu_b) increases as horizontal distance *X* increases and it becomes maximum at the right edge of the bottom wall due to the cooled right wall. Away from the walls and as *Ha* increases, the heat transfer rate decreases. For $Ha = 0$ and 10, due to the presence of secondary circulated cells in the right corner of the bottom wall and with opposite direction of the primary circulation, the heat transfer rate are oscillates in nature form $X = 0.65$ to 1. It is also observed that there is no significant effect on the heat transfer rate when the inclination angle (ϕ) is changed from 0 to $\pi/2$. Figure 8(b) shows the heat transfer rate at the left wall (Nu_l) oscillates with increasing the value of vertical distance *Y* for $Ha = 0$ and 10 and any value of ϕ. It is also note that the heat transfer rate at the right and top walls (Nu_r, Nu_t) in Figure 8(c) and (d) are symmetric about the center of the walls to the heat transfer rate at the left and bottom walls (Nu_l, Nu_b) in Figure 8(a) and (b), respectively.

Figure 9(a)-(d) shows the influence of the Hartmann number *Ha* and the magnetic field inclination angle ϕ on the average Nusselt numbers for the bottom, left, right and top walls, respectively. It is observed from Figure 11(a) and (b) that the average Nusselt numbers for the bottom and left walls decrease significantly as *Ha* increases for any inclination angel (ϕ). But the decreasing trend of average Nusselt number breaks at $Ha = 60$ for the left wall and it is increases slowly as *Ha* increases to 100. Since the local nusslet numbers Nu_r and Nu_t are symmetric to Nu_l and Nu_b which implies that

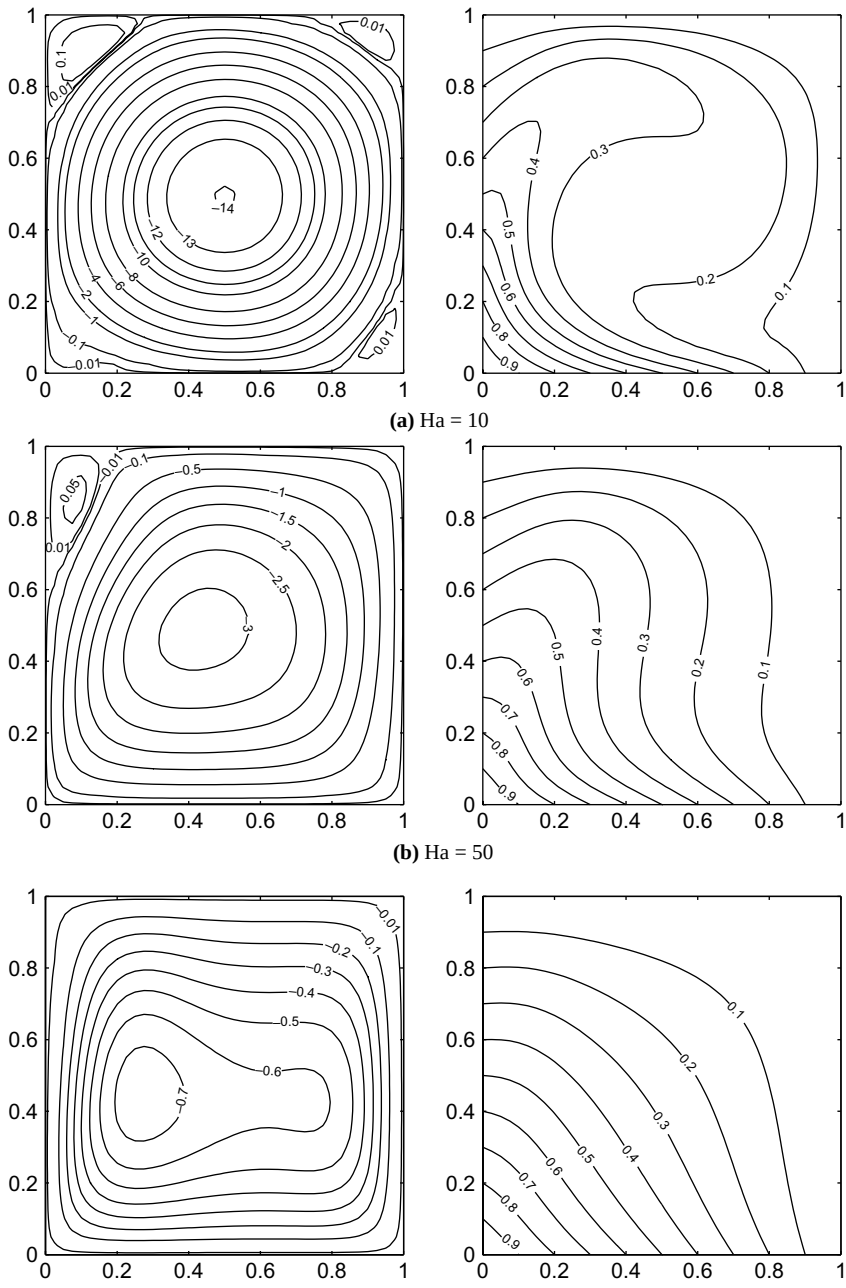

Figure 7.
Contour plots of linearly heated left and bottom walls under vertical magnetic field orientation

Note: $\phi = \pi/2$

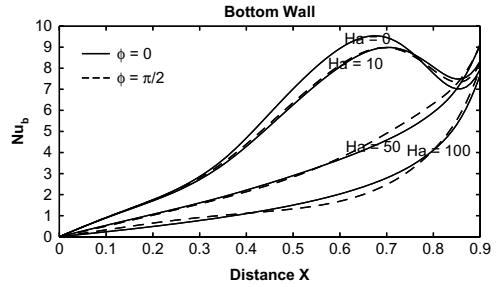

(a)

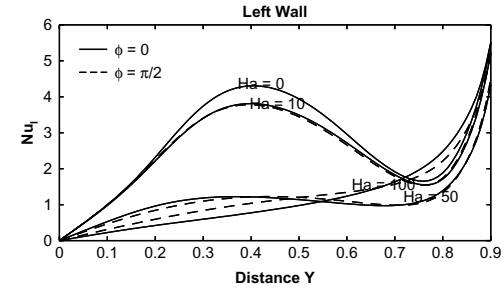

(b)

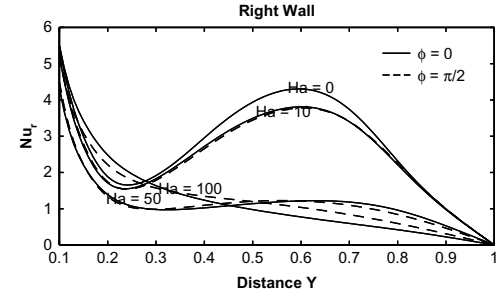

(c)

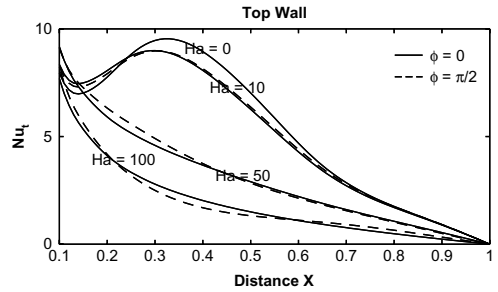

(d)

Notes: $Pr = 0.054$; $Ra = 10^5$

Figure 8.
Variation of local Nusselt number with distance at walls of the cavity for uniformly heated adjacent walls

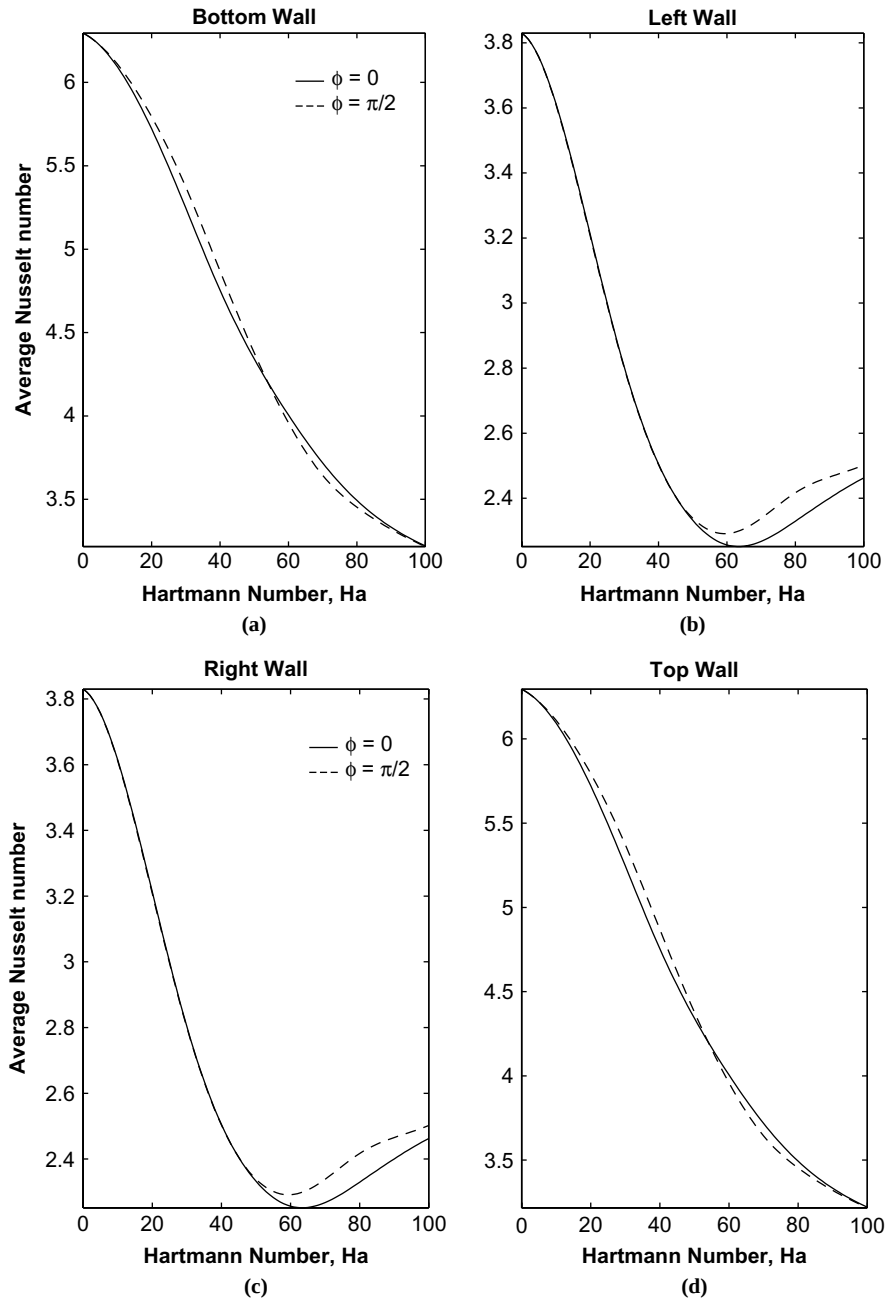

Figure 9.
Variation of average Nusselt number with Hartmann number *Ha* for uniformly heated adjacent walls

Notes: $Pr = 0.054$; $Ra = 10^5$

$\overline{Nu_r} = \overline{Nu_l}$ and $\overline{Nu_t} = \overline{Nu_b}$ as seen Figure 9, i.e. the overall heat transfer rates of the opposite walls are equal for uniformly heated adjacent walls.

2. Linearly heated adjacent walls. Figure 10 (a)-(d) display the effects of Ha and ϕ on the local Nusselt numbers at the bottom, left right and top walls (Nu_b, Nu_l and Nu_r) for linearly heated left wall and bottom wall, respectively. As seen Figure 10(a), the local Nusselt number Nu_b at the left edge of the bottom wall is 1 due to linearly heated left wall while it is 0 at right edge due to cooled right wall. At $Ha = 0$ and 10 for any inclination angle (ϕ), the heat transfer rate increases significantly as the horizontal distance X starting from 0 at the left-edge of the bottom wall towards the center with its maximum value at the center. In Figure 10(b), the heat transfer rate at the left wall (Nu_l) oscillates with the vertical distance Y. Also the length of oscillation, maximum and minimum values of the oscillation increases as Ha decreases. Figure 10(c) shows that the variation of local Nusselt number at the right wall oscillates naturally for low values of $Ha = 0$ and 10. For higher values of $Ha = 50$ and 100, the heat transfer rate for the horizontally-applied magnetic field ($\phi = 0$) is higher than the corresponding value for vertically applied magnetic field ($\phi = \pi/2$). The trend of the local Nusselt number at the top wall (Nu_t) in Figure 10(d) same as the trend of Nu_b that is discussed in Figure 10(a).

Finally, Figure 11(a)-(d) shows the influence of increasing Ha and ϕ on the average Nusselt numbers for the bottom, left, right and top walls for the case of linearly heated adjacent walls, respectively. It is predicted that the average Nusselt numbers at the bottom, right and top walls decrease significantly as Ha increases. However, the decreasing trend breaks at $Ha = 35$ for left wall and it has negative value in the range $20 \leq Ha \leq 40$ as seen in Figure 11(b). It is also observed that the average Nusselt number for the horizontally-applied magnetic field ($\phi = 0$) is higher than the corresponding value for vertically applied magnetic field ($\phi = \pi/2$) when $50 \leq Ha \leq 100$ for bottom wall while $20 \leq Ha \leq 100$ for right wall (Figure 11(a) and (c)). But the average Nusselt number at the top wall for the horizontally-applied magnetic field ($\phi = 0$) is lower than the corresponding value for vertically applied magnetic field ($\phi = \pi/2$) when $0 \leq Ha \leq 70$ as seen Figure 11(d). Contrary to the behavior of average Nusselt number shown in Figure 9 for uniformly heated adjacent walls, $\overline{Nu_r} \neq \overline{Nu_l}$ and $\overline{Nu_t} \neq \overline{Nu_b}$ for linearly heated adjacent walls as seen in Figure 11. But it is verified that the sum of the overall heat transfer rates of linearly heated the adjacent walls equal to the sum of overall heat transfer rates of the cooled adjacent walls, i.e. $\overline{Nu_b} + \overline{Nu_l} = \overline{Nu_r} + \overline{Nu_t}$.

5. Conclusions

The present study considered steady, laminar, two-dimensional MHD natural convection within a liquid metals filled square enclosure in the presence of inclined magnetic field for different thermal boundary conditions. The governing equations are developed and the solved by the penalty finite element method with bi-quadratic rectangular elements for the cases of uniformly or linearly heated bottom and left walls with cooled right and top walls. In both cases, the fluid rises up along the heated left wall and falls down along the cold right wall and it follows the path concentric circles which have center at center of the cavity. In general, the application of the magnetic field features different flow patterns respective of magnetic field's strength and inclined angle and it reduces the convective heat transfer rate in the cavity for any inclined angle. In addition, the local Nusselt number at the bottom wall of the cavity exhibited

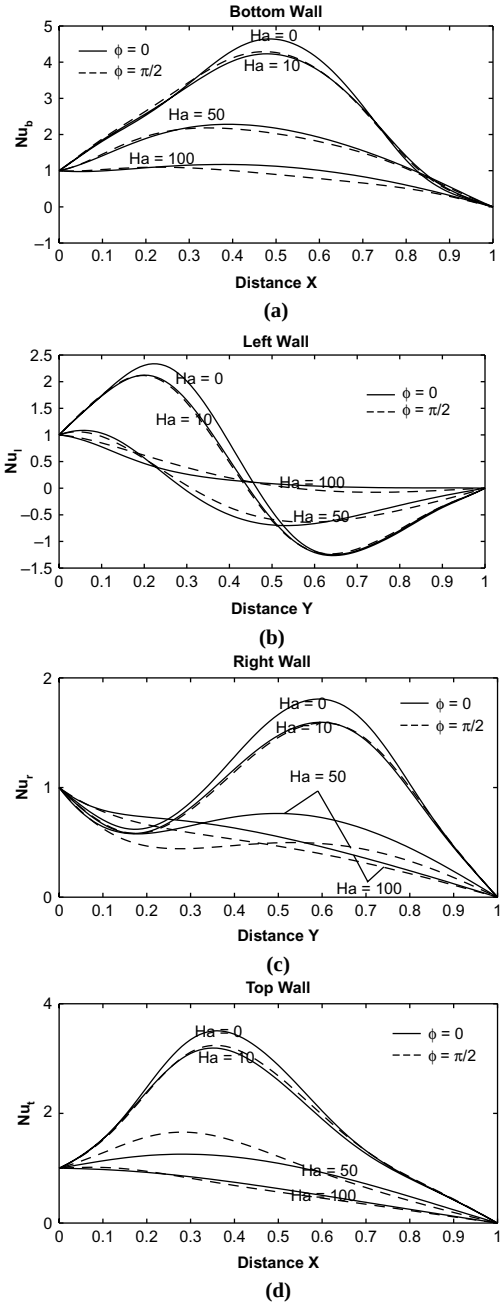

Figure 10.
Variation of local Nusselt number with distance at walls of the cavity for linearly heated adjacent walls

Notes: $Pr = 0.054$; $Ra = 10^5$

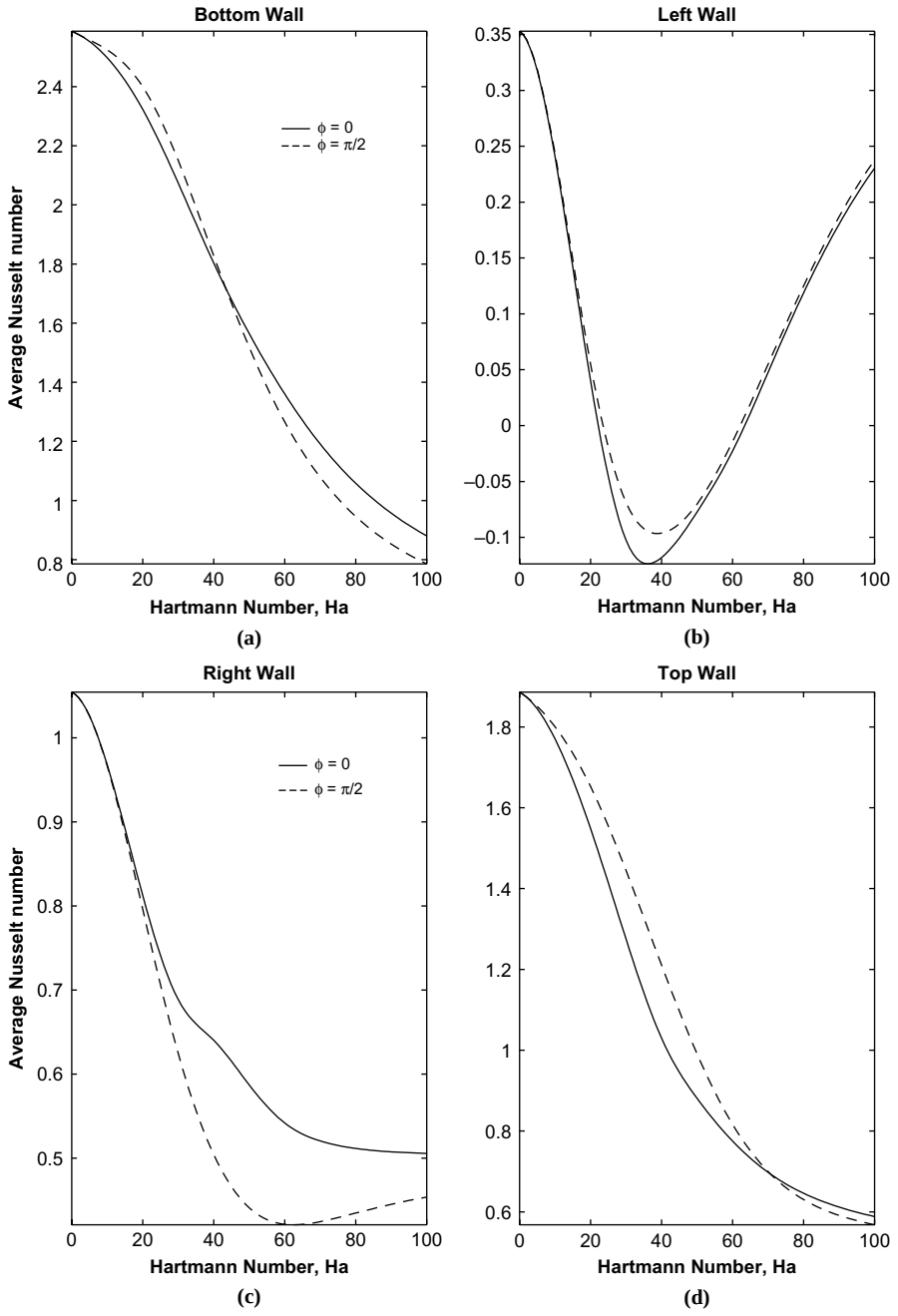

Notes: $Pr = 0.054$; $Ra = 10^5$

Figure 11.
Variation of average Nusselt number with Hartmann number *Ha* for linearly heated adjacent walls

oscillatory behavior along the horizontal distance for the both case of thermal boundary conditions. In general, the average Nusselt number decreases as *Ha* increases in the present study.

References

Alchaar, S., Vasseur, P. and Bilgen, E. (1995), "Natural convection heat trasnfer in a rectangular enclosure with transverse magnetic field", *Journal of Heat Trasnfer-Transations of the ASME*, Vol. 117, pp. 668-73.

Ece, M.C. and Buyuk, E. (2006), "Natural convection flow under magnetic field in an inclined rectangular enclosure heated and cooled on adjacent walls", *Fluid Dynamics Research*, Vol. 38, pp. 564-90.

Garandet, J.P., Albousseiere, T. and Moreau, M. (1992), "Bouyancy driven convection in a rectangular enclosure with a transverse magnetic field", *International Journal of Heat and Mass Transfer*, Vol. 35, pp. 741-8.

Kahveci, K. and Oztuna, S. (2009), "MHD natural convection flow and heat transfer in a laterally heated partitioned enclosure", *European Journal of Mechanics B/Fluids*, Vol. 28, pp. 744-52.

Kakarantzas, S.C., Sarris, I.E., Grecos, A.P. and Vlachos, N.S. (2009), "Magnetohydrodynamic natural convection in a vertical cylindrical cavity with sinusoidal upper wall temperature", *International Journal of Heat and Mass Transfer*, Vol. 52, pp. 250-9.

Kulacki, F.A., Davidson, P.F. and Dunn, J.H. (1987), "Convective heat transfer with electric and magnetic field", in Kakac, S., Shah, R.K. and Aung, W. (Eds), *Handbook of Single-Phase Convective Heat Transfer*, Wiley, New York, NY.

Mahmud, S. and Fraser, R.A. (2004), "Magnetohydrodynamic free convection and entropy generation in a square cavity", *International Journal of Heat and Mass Transfer*, Vol. 47, pp. 3245-56.

Mallinson, G.D. and Vahl Davis, G.D. (1977), "Three-dimensional natural convection in a box: a numerical study", *Journal of Fluid Mechanics*, Vol. 83, pp. 1-31.

Moreau, M. (1990), *Magnetohydrodynamics*, Kluwer Acadamic, Dordrecht The Netherlands.

Oreper, G.M. and Szekely, J. (1983), "The effect of an externaly imposed magnetic field on buoyancy driven flow in a rectangular cavity", *Journal of Cristal Growth*, Vol. 64, pp. 505-15.

Ozoe, H. and Maruo, E. (1987), "Magnetic and gravitational natural convection of melted silicon – two dimensional numerical computations for the rate of heat transfer", *J.S.M.E.*, Vol. 30, pp. 774-84.

Ozoe, H. and Okada, K. (1989), "The effect of the direction of the external magnetic field on the three-dimensional natural convection flow in a cubical enclosure", *International Journal of Heat and Mass Transfer*, Vol. 32, pp. 1939-54.

Oztop, H.F., Oztop, M. and Varol, Y. (2009), "Numerical simulation of magnetichydrodynamic buoyancy-induced flow in a non-isothermally heated square enclosure", *Communications in Non-linear Science and Numerical Simulation*, Vol. 14, pp. 770-8.

Pirmohammadi, M. and Ghassemi, M. (2009), "Effect of magnetic field on convection heat transfer inside a tilted square enclosure", *International Communications in Heat and Mass Transfer*, Vol. 36, pp. 776-80.

Reddy, J.N. and Gartling, D.K. (1994), *The Finite Element Method in Heat Transfer and Fluid Dynamics*, CRC-Press, Boca Raton, FL.

Rudraiah, N., Barron, R.M., Venkatachalappa, M. and Subbaraya, C.K. (1995), "Effect of magnetic field on free convection in a rectangular enclosure", *International Journal of Engineering Science*, Vol. 33, pp. 1075-84.

Sathiyamoorthy, M. and Chamkha, A. (2009), "Effect of magnetic field on natural convection flow in a liquid gallium filled square cavity for linearly heated side wall(s)", *International Journal of Thermal Sciences*, Vol. 49, pp. 1856-65.

Series, R.W. and Hurle, D.T.J. (1991), "The use of magnetic fields in semiconductor crystal growth", *Journal of Cristal Growth*, Vol. 133, pp. 305-28.

Sivasankaran, S., Malleswaran, A., Lee, J. and Sundar, P. (2011), "Hydro-magnetic combined convection in a lid-driven cavity with sinusoidal boundary conditions on both sidewalls", *International Journal of Heat and Mass Transfer*, Vol. 54, pp. 512-25.

Sreenivasan, B., Davidson, P.A. and Etay, J. (2005), "On the control of surface waves by a vertical magnetic field", *Physics of Fluids*, Vol. 17, p. 117101.

Utech, H.P. and Flemmings, M.C. (1966), "Elimination of solute banding in indium atimondic crystals by growth in a magnetic field", *Journal of Applied Physics*, Vol. 37, pp. 2021-4.

Venkatachalappa, M. and Subbaraya, C.K. (1993), "Natural convection in a rectangular enclosure in the presence of magnetic field with uniform heat flux from side walls", *Acta Mechanica*, Vol. 96, pp. 13-26.

Vives, C. and Perry, C. (1987), "Effects of magnetically damped convection during the controlled solidification of metals and ayylos", *International Journal of Heat and Mass Transfer*, Vol. 30, pp. 479-96.

Yang, K.T. (1987), "Natural convection in enclosures", in Kakac, S., Shah, R.K. and Aung, W. (Eds), *Handbook of Single-Phase Convective Heat Transfer*, Wiley, New York, NY.

Appendix

In the penalty finite element the pressure P that occurs in the momentum equations (5)-(6) is eliminated by both the penalty parameter γ and the incompressibility given in the equation (4) which results in:

$$P = -\gamma\left(\frac{\partial U}{\partial X} + \frac{\partial V}{\partial Y}\right). \tag{A1}$$

The continuity equation (4) is automatically satisfied for large value of γ. Typical values of γ that yield consistent solutions are 10^7 (Reddy and Gartling, 1994).

Using equation (AI), the momentum balance equations (5) and (6) reduce to:

$$U\frac{\partial U}{\partial X} + V\frac{\partial U}{\partial Y} = \gamma\frac{\partial}{\partial X}\left(\frac{\partial U}{\partial X} + \frac{\partial V}{\partial Y}\right) + Pr\left(\frac{\partial^2 U}{\partial X^2} + \frac{\partial^2 U}{\partial Y^2}\right) + PrHa^2(V\sin\phi\cos\phi - U\sin^2\phi) \tag{A2}$$

and:

$$U\frac{\partial V}{\partial X} + V\frac{\partial V}{\partial Y} = \gamma\frac{\partial}{\partial Y}\left(\frac{\partial U}{\partial X} + \frac{\partial V}{\partial Y}\right) + Pr\left(\frac{\partial^2 V}{\partial X^2} + \frac{\partial^2 V}{\partial Y^2}\right) + RaPr\theta \quad + PrHa^2(U\sin\phi\cos\phi - V\cos^2\phi) \tag{A3}$$

Expanding the velocity components (U,V) and temperature (θ) using basis set $\{\Phi_k\}_{k=1}^{N}$ as:

$$U \simeq \sum_{k=1}^{N} U_k \Phi_k(X,Y),\ V \simeq \sum_{k=1}^{N} V_k \Phi_k(X,Y),\ \theta \simeq \sum_{k=1}^{N} \theta_k \Phi_k(X,Y), \tag{A4}$$

for $0 \le X,Y \le 1$. The Galerkin finite element method yields the following nonlinear residual equations for equations (7), (A2) and (A3), respectively, at the nodes $i(1 \le i \le N)$ of internal domain Ω:

$$\begin{aligned} R_i^{(1)} = & \sum_{k=1}^{N} U_k \int_\Omega \left[\left(\sum_{k=1}^{N} U_k \Phi_k \right) \frac{\partial \Phi_k}{\partial X} + \left(\sum_{k=1}^{N} V_k \Phi_k \right) \frac{\partial \Phi_k}{\partial Y} \right] \Phi_i dXdY \\ & + \gamma \left[\sum_{k=1}^{N} U_k \int_\Omega \frac{\partial \Phi_i}{\partial X} \frac{\partial \Phi_k}{\partial X} dXdY + \sum_{k=1}^{N} V_k \int_\Omega \frac{\partial \Phi_i}{\partial X} \frac{\partial \Phi_k}{\partial Y} dXdY \right] \\ & + Pr \sum_{k=1}^{N} U_k \int_\Omega \left[\frac{\partial \Phi_i}{\partial X} \frac{\partial \Phi_k}{\partial X} + \frac{\partial \Phi_i}{\partial Y} \frac{\partial \Phi_k}{\partial Y} \right] dXdY \\ & - PrHa^2 \int_\Omega \left[\left(\sum_{k=1}^{N} V_k \Phi_k \right) \sin\phi\cos\phi - \left(\sum_{k=1}^{N} U_k \Phi_k \right) \sin^2\phi \right] \Phi_i dXdY \end{aligned} \tag{A5}$$

$$\begin{aligned} R_i^{(2)} = & \sum_{k=1}^{N} V_k \int_\Omega \left[\left(\sum_{k=1}^{N} U_k \Phi_k \right) \frac{\partial \Phi_k}{\partial X} + \left(\sum_{k=1}^{N} V_k \Phi_k \right) \frac{\partial \Phi_k}{\partial Y} \right] \Phi_i dXdY \\ & + \gamma \left[\sum_{k=1}^{N} U_k \int_\Omega \frac{\partial \Phi_i}{\partial Y} \frac{\partial \Phi_k}{\partial X} dXdY + \sum_{k=1}^{N} V_k \int_\Omega \frac{\partial \Phi_i}{\partial Y} \frac{\partial \Phi_k}{\partial Y} dXdY \right] \\ & + Pr \sum_{k=1}^{N} V_k \int_\Omega \left[\frac{\partial \Phi_i}{\partial X} \frac{\partial \Phi_k}{\partial X} + \frac{\partial \Phi_i}{\partial Y} \frac{\partial \Phi_k}{\partial Y} \right] dXdY \\ & - PrHa^2 \int_\Omega \left[\left(\sum_{k=1}^{N} U_k \Phi_k \right) \sin\phi\cos\phi - \left(\sum_{k=1}^{N} V_k \Phi_k \right) \cos^2\phi \right] \Phi_i dXdY \\ & - RaPr \int_\Omega \left(\sum_{k=1}^{N} \theta_k \Phi_k \right) \Phi_i dXdY \end{aligned} \tag{A6}$$

$$\begin{aligned} R_i^{(3)} = & \sum_{k=1}^{N} \theta_k \int_\Omega \left[\left(\sum_{k=1}^{N} U_k \Phi_k \right) \frac{\partial \Phi_k}{\partial X} + \left(\sum_{k=1}^{N} V_k \Phi_k \right) \frac{\partial \Phi_k}{\partial Y} \right] \Phi_i dXdY \\ & + \sum_{k=1}^{N} \theta_k \int_\Omega \left[\frac{\partial \Phi_i}{\partial X} \frac{\partial \Phi_k}{\partial X} + \frac{\partial \Phi_i}{\partial Y} \frac{\partial \Phi_k}{\partial Y} \right] dXdY, \end{aligned} \tag{A7}$$

where:

$$R_i^{(1)} = Pr \int_\Gamma \left(n_X \frac{\partial U}{\partial X} + n_Y \frac{\partial U}{\partial Y} \right) \Phi_i ds,\ \ R_i^{(2)} = Pr \int_\Gamma \left(n_X \frac{\partial V}{\partial X} + n_Y \frac{\partial V}{\partial Y} \right) \Phi_i ds,$$
$$R_i^{(3)} = \int_\Gamma \left(n_X \frac{\partial \theta}{\partial X} + n_Y \frac{\partial \theta}{\partial Y} \right) \Phi_i ds,$$

N is the number of nodes in the domain Ω and Γ is the boundary of the domain Ω. Bi-quadratic basis functions with three point Gaussian quadrature is used to evaluate the

integrals in the residual equations. In equations (A5)-(A6), the second term containing the penalty parameter (γ) are evaluated with two point Gaussian quadrature (reduced integration penalty formulation (Reddy and Gartling (1994)). The motivation for reduced integration follows is given below. The matrix vector notation the penalty finite element equations of the residuals, i.e. equations (A5)-(A6) may be expressed in matrix vector notation as:

$$(\mathbf{K}_1 + \gamma\mathbf{K}_2)a = \mathbf{F}, \tag{A8}$$

where $\mathbf{a}$ denotes the unknown vector, $\mathbf{K}_1$, $\mathbf{K}_2$ are the matrices obtained from the Jacobian of the residuals. As γ tends to a large value ($\sim 10^7$), the constraint equation (i.e. continuity equation) is satisfied better, which in turn causes the magnitude of $\mathbf{K}_1$ is negligible when compared with $\gamma\mathbf{K}_2$ resulting:

$$\mathbf{K}_2\mathbf{a} = \frac{\mathbf{F}}{\gamma}. \tag{A9}$$

This implies that as γ tends to infinity, governing equations are left with only the constraint condition, i.e. the continuity equation. Hence, the contributions from the momentum and energy conservations are completely lost. In addition, as $\mathbf{K}_2$ is nonsingular for large value γ the resulting solution obtained from equation (A9) is trivial. To obtain the non-trivial solutions for large $\gamma(\sim 10^7)$ the matrix $\mathbf{K}_2$ is needed to be a singular matrix. This is obtained by using two point Gaussian quadrature for $\mathbf{K}_2$ and three point Gaussian for $\mathbf{K}_1$. In the absence of the above reduced integration method velocities are underestimated (Reddy and Gartling, 1994).

The non-linear residual equations (A5)-(A6) are solved using a Newton-Raphson procedure to determine the coefficients of the expansions in equation (A4). At each iteration, the linear ($3N \times 3N$) system:

$$J(\mathbf{a}^n)[\mathbf{a}^n - \mathbf{a}^{n+1}] = \mathbf{R}(\mathbf{a}^n), \tag{A10}$$

is solved where n is iterative index. The element of the Jacobian matrix, $\mathbf{J}(\mathbf{a}^n)$ contains the derivatives of the residual equations with respect to velocity components (U_j)'s, (V_j)'s and the temperature (θ_j)'s and $\mathbf{R}(\mathbf{a}^n)$ is the vector of residuals. The linear system for each iteration is based on efficient node numbering of the elements such that the jacobian forms a banded matrix. The iterative process is terminated with the convergence criterion $\left[\sum\left(R_i^j\right)^2\right]^{0.5} \leq 10^{-5}$ using two-norm of residual vectors.

We have used nine node bi-quadratic elements which mapped using iso-parametric mapping (Reddy and Gartling (1994)) from X-Y to a unit square $\xi - \eta$ domain. Subsequently, the domain integrals in the residual equations are evaluated using nine node bi-quadratic basis functions in $\xi - \eta$ domain as:

$$X = \sum_{i=1}^{9} X_i\Phi_i(\xi, \eta),\ Y = \sum_{i=1}^{9} Y_i\Phi_i(\xi, \eta), \tag{A11}$$

where $\Phi_i(\xi,\eta)$ are the local bi-quadratic basis functions on the $\xi - \eta$ domain. The integrals in equations (A5)-(A6) can be evaluated in $\xi - \eta$ domain using following relationships:

$$\begin{bmatrix} \frac{\partial\Phi_i}{\partial X} \\ \frac{\partial\Phi_i}{\partial Y} \end{bmatrix} = \frac{1}{|J|}\begin{bmatrix} \frac{\partial Y}{\partial\eta} & -\frac{\partial Y}{\partial\xi} \\ -\frac{\partial X}{\partial\eta} & \frac{\partial Y}{\partial\xi} \end{bmatrix}\begin{bmatrix} \frac{\partial\Phi_i}{\partial\xi} \\ \frac{\partial\Phi_i}{\partial\eta} \end{bmatrix}$$

and:

$$dXdY = |J|d\xi d\eta \tag{A12}$$

were $J = \left|\partial(X, Y)/\partial(\xi, \eta)\right|$. The local Nusselt number on a surface (Nu) contains a normal derivative as shown in equation (11) and the normal derivative is evaluated using the bi-quadratic basis set in $\xi - \eta$ domain using equations (A11) and (A12).

Corresponding author
Ali J. Chamkha can be contacted at: achamkha@yahoo.com